Range-of-motion affects cartilage fluid load support: functional implications for prolonged inactivity

J.M. Benson[1], C. Kook[2], A.C. Moore[1], S. Voinier[2], C. Price[1], D.L. Burris[1,2]*
[1]Department of Biomedical Engineering
[2]Department of Mechanical Engineering
University of Delaware
Newark, DE

Abstract
Objective: Joint movements sustain cartilage fluid load support (*FLS*) through a combination of contact migration and periodic bath exposure. Although there have been suggestions that small involuntary movements may disrupt load-induced exudation during prolonged inactivity, theoretical studies have shown otherwise. This work used well-controlled explant measurements to experimentally test an existing hypothesis that the range-of-motion must exceed the contact length to sustain non-zero *FLS.*
Method: Smooth glass spheres (1.2 - 3.2 mm radius) were slid at 1.5 mm/s (Péclet number >100) against bovine osteochondral explants under varying normal loads (0.05 – 0.1 N) and migration lengths (0.05 - 7 mm) using a custom instrument. *In situ* deformation measurements were used to quantify *FLS*.
Results: Non-zero *FLS* was maintained at migration lengths as small as 0.05 mm or <10% the typical contact diameter. *FLS* was maximized when track lengths exceeded 10 times the contact diameter. For migration lengths below this threshold, *FLS* decreased with increased contact stress.
Conclusions: Migration lengths far smaller than the contact diameter can sustain non-zero *FLS*, which, from a clinical perspective, indicates that fidgeting and drifting might mitigate exudation and loss of *FLS* during prolonged sitting and standing. Nonetheless, *FLS* decreased monotonically with decreased migration length when migration lengths were less than 10 times the contact diameter. The results demonstrate: (1) potential biomechanical benefits from small movement (e.g. drifting and fidgeting); (2) the quantitative limits of those benefits; (3) and how loads, movement patterns, and mobility likely impact long term *FLS*.

keywords: Cartilage; joint range of motion; fidgeting; fluid load support; contact migration

***corresponding author**
David L. Burris, Ph.D.
Dept. of Mechanical Engineering
University of Delaware
dlburris@udel.edu
(302) 831-2006

1.0 Introduction

One of the first and most influential cartilage mechanics studies was conducted by McCutchen, who slowly slid cartilage plugs against smooth flat glass and quantified both friction and deformation[1]. In this, and other similar studies[2–4], friction coefficients initially fell below 0.01 in both 'good' (synovial fluid) and 'poor' (water) lubricants, but increased to well over 0.3 as the tissue deformed due to time-dependent interstitial fluid loss. As a result of these findings, McCutchen proposed that large stores of hydrostatically pressurized interstitial fluid preferentially supported the load and, as a result, reduced friction; the fraction of the load supported by hydrostatically pressurized interstitial fluid has been defined as fluid load support (*FLS*)[5,6].

Despite its functional benefits, load induced interstitial pressurization ultimately drives fluid from the contact, defeating interstitial pressure, *FLS*, and lubrication over time[1,5]. Based on typical joint stresses and contact areas, significant fluid losses (i.e., strains) on the order of 30-50% are both expected and observed over just a few hours of static loading[7,8]. However, there is no evidence that interstitial hydration and *FLS* are lost to this degree when joints are free to move *in vivo*. Instead, *in vivo* joint space measurements demonstrate that interstitial hydration is maintained throughout a typical day. For example, Coleman *et al.* showed that cartilage in the human knee thins by only 1-5% over an average day while Eckstein *et al.* showed no time-dependent fluid loss (i.e. thinning) during an hour of exercise[9,10].

It has been suggested that the long-term maintenance of interstitial fluid and *FLS* can be explained by the migrating contact area (MCA)[3,5,11]. According to this theory, the MCA halts exudation by moving the contact area across the cartilage surface faster than the exudative speed of the interstitial fluid[3,11]. Furthermore, the periodic unloading of the surface due to contact area migration enables periodic free-swelling[1,12,13]. Theoretical[11,14,15] and experimental[3,4,6,16] studies have consistently shown that cartilage retains high *FLS* if the contact continues to migrate over sufficient distances and at sufficient speeds to limit or reverse load-induced fluid exudation.

Contact migration fails to explain why joint space and *FLS* are sustained despite periods of inactivity, which comprises most of the waking day for most adults[17–19]. One hypothesis is that the joint slowly loses interstitial fluid while the body maintains static occupational and leisure-time positions, but quickly recovers lost interstitial fluid and *FLS* during subsequent movement prior to joint space measurements[5,20,21]. In light of existing literature on cartilage biomechanics and tribology[1–3,22,23], this hypothesis suggests that joints may be exposed to brief periods of very high friction during movement prior to full recovery, which could increase the risk of permanent cartilage damage and joint dysfunction[24,25]. An alternate hypothesis is that subtle unintentional movements (*e.g.* drifting, shifting, and fidgeting)[26,27] help sustain the MCA and its benefits to joint biomechanics, even during periods of nominal inactivity. A similar hypothesis was first proposed by Lewis and McCutchen after noting that animals that sleep standing up reposition themselves at least every half hour[28].

This small movement hypothesis is consistent with clinical observations that: (1) joint space is largely maintained throughout the day despite varying inactivity within cohorts[9], and (2) risk of

joint disease only increases slightly (albeit significantly) in the least active populations after correcting for body mass (or BMI)[29–32]. However, it appears to lack support from our current understanding of basic cartilage biomechanics. Results from a biphasic finite element model showed that the MCA failed to produce significant *FLS* when the contact diameter exceeded the stroke length because, as the authors note, the majority of the contact area was 'always loaded'[15]. This interpretation implies that small joint movements are also unable to sustain *FLS* if they fail to unload the majority of the contact area.

The variation in *FLS* with decreasing migration length, particularly as it approaches the contact length, has yet to be studied experimentally. This paper aimed to fill this clinically significant knowledge gap. We used well-controlled MCA explant experiments with *in situ FLS* measurements[4,6,16,33] to: (1) systematically quantify the relationships between contact migration length, stress, and *FLS* in bovine articular cartilage; (2) incorporate the measured migration length effect into existing biphasic theory; (3) highlight the most important biomechanical and clinical implications of the findings, especially with regards to anticipated range-of-movement magnitudes within the joint *in vivo*.

2.0 Methods

2.1 Experimental details

This study used N=5 full thickness osteochondral plugs from the femoral condyles of 3 mature bovine stifles from 3 different animals. The ϕ19 mm samples were extracted with a coring drill, rinsed in 1X phosphate buffered saline (PBS), stored in PBS containing 1X protease inhibitor (Sigma-Aldrich, P8340) at 4°C, and tested within 24 hours.

Migrating contact area (MCA) measurements were made using the custom indenter shown in Figure 1A with previously developed methods[6]. Samples were mounted to the reciprocating stage and then tilted to align the surface normal to the vertical axis. Smooth (average roughness < 100 nm), impermeable, glass spheres of varying size were indented and slid relative to the cartilage. The contact force (F) and penetration depth (δ) were controlled via a nanopositioning stage (PI USA, P-6.821CL; 0-800 ± 0.01 μm) and sliding motions were controlled with a stepper-driven linear stage (mDrive NEMA17; 0-20 ± 0.005 mm).

Immediately prior to sliding, the sample was indented at 50 μm/s to a target stage position. The contact force and penetration depth were recorded continuously until the sample reached equilibrium, which we defined as a mean rate-change in penetration depth of less than 0.3 μm/min. The time, load, and penetration depth results were fit to obtain the tensile modulus (E_t), equilibrium contact modulus (E_{c0}) and permeability (k) as described previously[16,34]; the fitting code and instructions can be downloaded from our website: http://research.me.udel.edu/~dlburris/HBTindent.html.

Immediately following static equilibration, the lateral stage was reciprocated at V = 1.5 mm/s over an S = 7 mm long migration length. Initially, fluid recovery exceeded fluid loss, resulting in

increased force and decreased penetration depth with time (see Figure 2A). The rate of net recovery slowed over time until reaching a dynamic equilibrium (defined by <0.3 μm/min change in penetration depth). Following dynamic equilibration, the migration length was reduced to 4 mm and the system was allowed to reach a new dynamic equilibrium. This procedure was repeated for 2, 1, 0.5, 0.2, 0.1, and 0.05 mm track lengths, in that order, for a given set of conditions. Each sample was subjected to this procedure at three target stage positions (20, 50, or 100 μm below first contact) and three probe sizes (ϕ 2.4, 3.9, 6.4mm) to vary contact force, contact stress, and contact area. The order in which indentation depth and probe diameter were tested in each sample was randomized. A definition of all terms is given in Table 1.

2.2 Theoretical Framework

The existing theoretical work on interstitial pressure and *FLS* in the MCA considers an effectively infinite migration length in which all areas of the cartilage surface are unloaded long enough between contacts to fully recover the fluid lost during the previous cycle (Figure 1B)[3,5,11]. FLS_{max} represents *FLS* of an effectively infinite track and depends on cartilage matrix material properties and sliding speed[16]:

$$FLS_{max} = \left(\frac{E_t}{E_t+E_{c0}}\right)\cdot\left(\frac{V\cdot a}{V\cdot a+E_{c0}\cdot k}\right) = \left(\frac{E_t}{E_t+E_{c0}}\right)\cdot\left(\frac{Pe}{Pe+1}\right) \quad \text{Eq. 1}$$

where $Pe\ (Peclet\ number) = V\cdot a/(E_{c0}\cdot k)$, V is sliding speed, a is the contact radius, E_{c0} is the equilibrium contact modulus, E_t is the tension modulus, and k is permeability[3,5,11,16]. Each term in this two-term equation limits *FLS*. For a linearly elastic biphasic material ($E_t = E_{c0}$), the elasticity term ($\frac{E_t}{E_t+E_{c0}}$) limits *FLS* to a maximum value of 50%[35,36]. For cartilage, $E_t >> E_{c0}$ and the elasticity-term is typically closer to 100%[33,34,37]. The second term, the migration term ($\frac{Pe}{Pe+1}$), relates the migration rate to the exudation rate. With V = 1.5 mm/s, Pe > 100 for every measurement in this study, which implies that the rate-term is effectively 100% (>99%) under all conditions.

For finite migration lengths, *FLS* is less than FLS_{max} and depends on the balance between fluid loss during contact and recovery between contacts. As Figure 1B illustrates, the loaded area or contact area ($A_c = \pi\cdot a^2$) loses fluid, on average, at a characteristic exudation rate (R_{ex}). The unloaded area or migration area ($A_m = S\cdot 2a = S\cdot d$) recovers fluid, on average, at a characteristic recovery rate (R_{rec}). Under arbitrary conditions, the system loses or gains fluid until the fluid lost balances the fluid recovered over the cycle period (t_{cycle}). Therefore, *FLS* can be expressed mathematically by Eq. 2, where A^* and R^* are the relative migration area and the exudation ratio, respectively, as defined in Table 1.

$$FLS = FLS_{max}\cdot\left(\frac{A_m\cdot R_{rec}\cdot t_{cycle}}{A_m\cdot R_{rec}\cdot t_{cycle}+A_c\cdot R_{ex}\cdot t_{cycle}}\right) = FLS_{max}\cdot\left(\frac{A^*}{A^*+R^*}\right) \quad \text{Eq. 2}$$

Solving this equation in terms of contact diameter and migration length (or the relative migration length, $S^*=S/d$) gives:

$$FLS = FLS_{max} \cdot \left(\frac{S \cdot d \cdot R_{rec} \cdot t_{cycle}}{S \cdot d \cdot R_{rec} \cdot t_{cycle} + \frac{\pi}{4} d^2 \cdot R_{ex} \cdot t_{cycle}} \right) = FLS_{max} \cdot \left(\frac{S^*}{S^* + \frac{\pi}{4} \cdot R^*} \right) \quad \text{Eq. 3}$$

Substituting Eq. 1 into right hand side of Eq. 3 gives a practical overall expression for *FLS* in terms of measurable quantities (material properties, sliding speed, contact diameter, and track length):

$$FLS = \left(\frac{E_t}{E_t + E_{c0}} \right) \cdot \left(\frac{V \cdot a}{V \cdot a + E_{c0} \cdot k} \right) \cdot \left(\frac{S}{S + 0.79 \cdot d \cdot R^*} \right) \quad \text{Eq. 4}$$

Eq. 4 implies that *FLS* is 50% FLS_{max} when fluid recovery occurs at the same rate and over the same area as fluid loss (R^*=1 by definition, and $S = 0.79 \cdot d$). At this condition, the center of the migration track (the location of measurement) experiences continuous loading and has no opportunity for direct recovery from the bath. The equation also implies that cartilage is capable of supporting *FLS* despite restricted migration ($S < d$ or $S^* < 1$) if the exudation rate is much slower than the recovery rate ($R^* << 1$). Given that the contact interface impedes exudation without affecting recovery into free surface, this framework, unlike prior biphasic analysis[15], describes how significant *FLS* can be sustained at vanishing ranges of motion.

2.3 Data analysis

The equilibrium *FLS* support was quantified for each test condition using *in-situ* force and penetration depth measurements as described previously[16,34]. It is important to note that these measurements were made at the center of the migration track (0 ± 0.005 mm), which is the location of indentation measurements for material characterization (location 1 in Figure 1C). The raw force and displacement measurements from a representative experiment are shown in Figure 2a for illustration. Mean results were taken from the first 10 cycles following the establishment of static (S = 0 mm) and dynamic equilibria (S = 7 – 0.05 mm).

On the basis that prior results support the use of Hertzian contact mechanics in small MCAs[4,6,38], the contact radius (a) is the following function of probe radius (R) and penetration depth (δ)[39]:

$$a = \sqrt{R\delta} \quad \text{Eq. 5}$$

The mean contact stress (σ) is the contact force (F) divided by the contact area (A_c). Thus, the effective contact modulus is a function of load, probe radius, and contact radius:

$$E_c = \frac{3}{4} \frac{F}{R^{0.5} \cdot \delta^{1.5}} = \frac{3}{4} \frac{F \cdot R}{a^3} \quad \text{Eq. 6}$$

FLS is a function of the equilibrium contact modulus (E_{c0}), measured during static loading, and the effective contact modulus (E_c), measured during sliding at dynamic equilibrium[16]:

$$FLS = 1 - \frac{F_{solid}}{F} = 1 - \frac{\frac{4}{3} \cdot E_{c0} \cdot R^{0.5} \cdot \delta^{1.5}}{\frac{4}{3} \cdot E_c \cdot R^{0.5} \cdot \delta^{1.5}} = 1 - \frac{E_{c0}}{E_c} \quad \text{Eq. 7}$$

To remove the material-dependent terms (which are known to vary significantly between samples[33]) and to study the migration length-dependent term in isolation, we define *relative FLS* as $F^* = FLS/FLS_{max}$. The baseline FLS_{max} measurement is derived from the corresponding 7 mm

migration length measurement and V = 1.5 mm/s. The normalizing effect on the results are illustrated in Figure 3.

Finally, F^* was plotted against S^* and fit to Eq. 3 to obtain the exudation ratio (R^*). Linear regressions were used to determine if R^* increases with increased contact stress or area. The statistical analysis was performed using JMP® Pro 14.0 and significant effects correspond to slopes with $p < 0.05$.

3.0 Results

Raw time-dependent force and penetration depth measurements from a representative migration experiment are shown in Figure 2A. For the initial static indention (0 mm track length), the force decreased, and the penetration depth increased over time until both reached equilibrium. Subsequent sliding along a 7 mm migration length caused the force to increase and the penetration depth (at the center of the migration track) to decrease due to interstitial pressurization until the system reached a dynamic equilibrium. The effective contact modulus, contact area, and contact stress were quantified based on these measurements and plotted against time in Figure 2B. For this representative experiment, the effective contact modulus increased from ~0.3 MPa at static equilibrium to ~3 MPa at dynamic equilibrium for an effectively infinite migration length. This increase in effective modulus/stiffness reduced the contact area by >50% and increased the contact stress by >4-fold. Reduced migration lengths led to systematically decreased contact modulus, decreased contact stress, and increased contact area.

The mean effective contact modulus, contact area, and contact stress are plotted as functions of migration length for representative measurements of three independent samples (lowest, median, highest contact stiffness) in Figure 3A-C. The variations observed between samples are typical of healthy bovine cartilage[33,34,38]. The effective contact modulus of sample 5 was about 50% lower than that of sample 1 (Figure 3A), which led to increased contact area (Figure 3B), and decreased contact stress (Figure 3C). However, these differences between samples effectively vanished when the *FLS* was normalized by FLS_{max} and plotted against relative migration length ($S^*=S/d$), as illustrated in Figure 3D. For all three samples, F^* varied with S^* as described by Eq. 3. In all three cases, *FLS* decreased by ~5% at S^* ~ 4 and ~12% at S^* ~ 2. Individual fits indicate an R^* between 0.15 and 0.22; *i.e.* exudation rates were ~15-22% the recovery rates at equilibrium. The material properties of all five samples are provided in Table 2.

The relative *FLS* (F^*) is plotted versus relative migration length (S^*) in Figure 4 for all 360 measurements in the study (5 samples x 8 tracks x 3 loads x 3 probe radii) – measurements are shaded according to sample number. Reductions in the migration length had no effect on *FLS* when $S^*>10$; *i.e.* the migration length is effectively 'infinite' and its effects can be ignored when the migration length exceeds the contact diameter by 10-fold. *FLS* decreased systematically with decreasing migration length when $S^*<10$. When the migration length matched the contact diameter ($S^*=1$), the experimentally observed loss of *FLS* averaged ~15%. Based on the fit, *FLS* decreased

by 50% at $S^* = 0.11$, which suggests that the exudation rate was ~14% the recovery rate on average (see Eq. 3).

Fitting the variable migration length experiments individually (as in Figure 3D) yielded exudation ratio values (R^*) that reflect the properties of the sample and the conditions of the experiment (3 loads x 3 probes). The fit values of R^* from each variable track measurement (3 x 3 x 5 samples) were plotted against contact stress and contact area in Figures 5A and 5B, respectively, to assess whether contact stress and contact area have systematic effects on exudation rates. Overall, R^* increased significantly with contact stress (0.32 MPa^{-1}, $p < 0.0001$) but not with contact area ($p = 0.06$).

4.0 Discussion

This experimental study resolves how restricted range-of-motion movements affect cartilage *FLS* and biomechanics. One key finding is that the cartilage in the center of restricted migration tracks (those with $S^* < 1$) can sustain meaningful *FLS* despite being subjected to uninterrupted contact and exudation stress. On average, we observed 50% of peak *FLS* ($F^* = 0.5$) when $S^* = 0.11$; at this condition, the central ~85% of the contact area was 'always loaded'. This observation is in contrast to biphasic modeling results showing that cartilage MCAs under similar contact areas, stresses, migration lengths, and migration speeds (d = 3.6 mm, σ = 250 kPa, S = 0.8 mm, V = 4 mm/s) sustained no *FLS* at $S^* \sim 0.22$[15]; *i.e.* the biphasic model fails to anticipate our primary experimental finding that cartilage MCAs can sustain meaningful *FLS* when the contact diameter significantly exceeds the migration length. Experimentally, we found that cartilage sustained between 50% and 90% *FLS* (F^*) at $S^* \sim 0.22$ for every sample, load, and probe radius in the study (Figure 4). Unlike traditional biphasic analysis, our theoretical framework does anticipate our findings and suggests that recovery rates exceeded exudation rates by ~3.5x; this is reasonable since the contact interface impedes exudation rates but not recovery rates.

A second key finding is that *FLS* is only independent of the migration length when the migration length is greater than 10-fold the contact diameter ($S^* > 10$). For studies that do not meet this criterion, the effect of migration length on *FLS* can be estimated using Eq. 3. Our first *in situ* study of *FLS* in MCAs failed this test, providing an excellent case study[6]. In that study, the measured contact radius and *FLS* for our 6.4 mm diameter probe were 0.247 mm ($S^* = 3.04$) and 88.4%, respectively; the measured contact radius and *FLS* for our 1.6 mm diameter probe were 0.137 mm ($S^* = 5.47$) and 91.1%, respectively. Using Eq. 3 with measured migration lengths, contact radii, and *FLS* indicates that the presence of restricted migration reduced *FLS* by 4.4% and 2.5% for the large (FLS_{max} = 91.6%) and small (FLS_{max} = 92.9%) probes, respectively. Thus, measured differences in *FLS* between probes were mostly due to differences in relative migration length, the effect of which we were unaware of at the time.

For MCA studies lacking *in situ FLS* measurements, Eq. 4 can be used to estimate or predict *FLS*. In the first controlled MCA experiments, Caligaris and Ateshian used a 36 mm diameter probe,

6.3 N load, 10 mm migration length, and 1 mm/s sliding speed[4]. Using these conditions with typical material properties (E_{c0} = 0.5 MPa, E_t = 5 MPa, and k = 0.001 mm^4/Ns) to solve Eqs. 4, 6, and 7 simultaneously provides a unique solution: FLS = 85.4%, E_c = 3.43 MPa, a = 2.92 mm. Our prior model[16], which neglected the restricted migration effect (S^*=1.65), over-predicts FLS by 6% (FLS_{max} = 90.9%); more importantly, it under-predicts solid stress and interfacial friction by 37% (9.1% vs 14.6%). This simple analytical framework can easily be applied to the analysis of existing literature and the design of experiments that better represent clinically relevant conditions. We are unaware of another theoretical approach that provides quantitatively valid estimates of MCA FLS, contact area, and contact stress.

In vivo, relative migration lengths during full range-of-motion are well below 10. Linn estimated that the range of canine ankle motion[12] corresponds to $S^* \sim 1$. Likewise, the human hip appears to have a similar migration environment; migration lengths (S)[40] and contact lengths (d)[41] both appear to be on order of 20-30 mm during walking. Given our current findings, these facts are disconcerting without further analysis. As Eq. 3 indicates, the system depends primarily on R^*, which varies in predictable ways with contact stress and area. According to biphasic theory[8,16,42], exudation rates increase proportionally with contact stress and inversely with contact area (the results in Figure 5 gave no significant evidence to the contrary). Given that contact stresses and contact areas in the hip[41] are ~10-fold and ~100-fold greater, respectively, than those in this study, we expect a net ~10-fold reduction of R^* to ~0.014 for the hip (recovery rates are unaffected by area and stress since they occur at free surfaces). Thus, the anticipated detrimental effect of $S^* \sim 1$ on FLS in the hip is only ~1% (F^* = 98.9%); this outcome is consistent with experimental observations of extraordinarily low strains and friction in human and animal joints[9,12,43,44].

An especially important open question grounded in the present work is the extent to which joints lose interstitial hydration and pressure during prolonged inactivity, which is a common occupational hazard[27]. FLS can be seriously compromised by just a few hours of truly static loading[7], but we know that even inactive human subjects engage in regular small-range-of-motion movements[26]. During prolonged unconstrained standing, standing at attention for example, the body's center of pressure may move by ~25 mm as we fidget (fast 'pulse-like'), shift (fast 'step-like') or drift (slow 'ramp-like')[26,45]. Assuming a 920 mm long leg and a 25 mm femoral head radius, such movements correspond to a hip articulation of ~1.5º and a migration length of ~0.7 mm. Using a contact length of 10 mm in the medial-lateral direction across the femoral head[41] yields $S^* \sim 0.07$. Applying $R^* \sim 0.014$ as before suggests that these small unconscious movements might generate ~80% peak FLS (FLS_{max}), which is a surprising and potentially critical clinical insight from this study.

A related question is whether peak FLS from such small movements is significant given their slow speeds. According Duarte *et al.*[45], shifting and fidgeting typically occur over ~1s durations, which corresponds to a migration speed of ~0.7 mm/s. Although this is quite slow compared to walking speeds (~50 mm/s)[20], it produces $Pe \sim$ 10,000 (assuming typical material properties) and has no

significant detrimental effect on the speed term of Eq. 4 (99.99%). However, neither is likely to sustain *FLS* since they only occur about 1% of the time[26,45]. Drifting is far slower (~7 μm/s) than shifting or fidgeting but it appears to be persistent. Even drifting's slow speeds produce $Pe \sim 100$, which effectively maximizes *FLS* (the speed term in Eq. 4 is 99.3%). Thus, after accounting for the migration effect, we can expect drifting to sustain *FLS* at ~80% its peak value. Drifting provides a clinically testable hypothesis[46–48] (the first that we are aware of) to help explain why joint space is so well regulated in highly variable *in vivo* environments[9,10,46].

Despite the optimism of these results, it must be kept in mind that even modest reductions in *FLS* can carry a heavy frictional cost. Direct SCA measurements from Krishnan *et al*. showed that purely interfacial friction more than doubled when *FLS* decreased by 20%[49]. Direct MCA measurements[3,6] by our group and others have shown that friction can more than triple for the same 20% reduction in *FLS;* although the magnitude of the friction force depends on the lubricant and contact geometry (i.e. plowing friction), the multiplicative effect of lost *FLS* on friction does not. Thus, while small involuntary movements may mitigate exudation to a surprising degree, reduced activity may still be accompanied by increased friction, increased potential for cartilage damage[25,50], and increased risk of joint disease[29–32]. These observations are consistent with and supportive of archeological and epidemiological studies suggesting connections between excessive inactivity and modest increases in joint disease risk[29,51,52]. Our hypothesis that small involuntary movements mitigate static exudation could explain why the added risk of OA in the least active populations studied, while significant, is rather small[29]. It may likewise explain why the >20% cartilage strains so commonly 'encountered' *ex-vivo*[1,7,49,53,54] appear to be quite rare *in vivo*[9,10,44,46,55,56].

In summary, i) we show the first direct evidence that movements far smaller than the dimensions of the migrating contact area can and do sustain non-zero *FLS*; ii) we developed and validated an analytical model describing this response; iii) we apply existing theory to extend the results to *in vivo* situations; iv) we demonstrate that small unintentional movements of healthy subjects during sedentary periods are likely to contribute to the long-term retention of interstitial hydration, pressure, and lubrication, and thus joint function and longevity.

6.0 Contributions of authors

The author contributions are as follows: (1) the conception and design of the study, or acquisition of data, or analysis and interpretation of data – JB, CK, AM, DB; (2) drafting the article or revising it critically for important intellectual content - JB, AM, SV, CP, DB; (3) final approval of the version to be submitted - JB, CK, AM, SV, CP, DB

7.0 Role of funding source

Funding for this research was provided by the NSF Biomaterials and Mechanobiology Program under award numbers BMMB-1635536 and BMMB-1937493. The NSF played no role in the

study design, collection, analysis and interpretation of data; in the writing of the manuscript; or in the decision to submit the manuscript for publication.

8.0 Competing Interests

The authors have no competing interests to report.

9.0 Acknowledgements

The authors gratefully acknowledge financial support from the NSF (NSF BMMB-1635536 and BMMB-1937493) for the development the theoretical and experimental methods for this study.

8.0 References

(1) McCutchen, C. W. The Frictional Properties of Animal Joints. *Wear* **1962**, *5*, 1–17.

(2) Forster, H.; Fisher, J. The Influence of Loading Time and Lubricant on the Friction of Articular Cartilage. *Proc. Inst. Mech. Eng. Part H-Journal Eng. Med.* **1996**, *210*, 109–119.

(3) Caligaris, M.; Ateshian, G. a. Effects of Sustained Interstitial Fluid Pressurization under Migrating Contact Area, and Boundary Lubrication by Synovial Fluid, on Cartilage Friction. *Osteoarthr. Cartil.* **2008**, *16*, 1220–1227.

(4) Moore, A. C.; Schrader, J. L.; Ulvila, J. J.; Burris, D. L. A Review of Methods to Study Hydration Effects on Cartilage Friction. *Tribol. - Mater. Surfaces Interfaces* **2017**, *5831*, 1–12.

(5) Ateshian, G. A. The Role of Interstitial Fluid Pressurization in Articular Cartilage Lubrication. *J. Biomech.* **2009**, *42* (9), 1163–1176.

(6) Bonnevie, E. D.; Baro, V.; Wang, L.; Burris, D. L. In-Situ Studies of Cartilage Microtribology: Roles of Speed and Contact Area. *Tribol. Lett.* **2011**, *41* (1), 83–95.

(7) Herberhold, C.; Faber, S.; Stammberger, T.; Steinlechner, M.; Putz, R.; Englmeier, K. H.; Reiser, M.; Eckstein, F. In Situ Measurement of Articular Cartilage Deformation in Intact Femoropatellar Joints under Static Loading. *J. Biomech.* **1999**, *32*, 1287–1295.

(8) Armstrong, C. G.; Lai, W. M.; Mow, V. C. An Analysis of the Unconfined Compression of Articular-Cartilage. *J. Biomech. Eng. Asme* **1984**, *106* (2), 165–173.

(9) Coleman, J. L.; Widmyer, M. R.; Leddy, H. A.; Utturkar, G. M.; Spritzer, C. E.; Moorman, C. T.; Guilak, F.; DeFrate, L. E. Diurnal Variations in Articular Cartilage Thickness and Strain in the Human Knee. *J. Biomech.* **2013**, *46* (3), 541–547.

(10) Eckstein, F.; Lemberger, B.; Gratzke, C.; Hudelmaier, M.; Glaser, C.; Englmeier, K.-H.; Reiser, M. In Vivo Cartilage Deformation after Different Types of Activity and Its Dependence on Physical Training Status. *Ann. Rheum. Dis.* **2005**, *64* (2), 291–295.

(11) Ateshian, G. A.; Wang, H. A Theoretical Solution for the Frictionless Rolling Contact of Cylindrical Biphasic Articular Cartilage Layers. *J. Biomech.* **1995**, *28* (11), 1341–1355.

(12) Linn, F. C. Lubrication of Animal Joints. I. The Arthrotripsometer. *J. bone Jt. Surg. Am. Vol.* **1967**, *49* (6), 1079–1098.

(13) Maroudas. The Permeability of Articular Cartilage. *J. bone Jt. Surg.* **1968**, *50 B* (1), 166–177.

(14) Accardi, M. A.; Dini, D.; Cann, P. M. Experimental and Numerical Investigation of the Behaviour of Articular Cartilage under Shear LoadingInterstitial Fluid Pressurisation and Lubrication Mechanisms. *Tribol. Int.* **2011**, *44* (5), 565–578.

(15) Pawaskar, S. S.; Jin, Z. M.; Fisher, J. Modelling of Fluid Support inside Articular

Cartilage during Sliding. *Proc. Inst. Mech. Eng. Part J J. Eng. Tribol.* **2007**, *221* (3), 165–174.
(16) Moore, A. C.; Burris, D. L. An Analytical Model to Predict Interstitial Lubrication of Cartilage in Migrating Contact Areas. *J. Biomech.* **2014**, *47* (1), 148–153.
(17) Pandey, A.; Salahuddin, U.; Garg, S.; Ayers, C.; Kulinski, J.; Anand, V.; Mayo, H.; Kumbhani, D. J.; De Lemos, J.; Berry, J. D. Continuous Dose-Response Association between Sedentary Time and Risk for Cardiovascular Disease a Meta-Analysis. *JAMA Cardiol.* **2016**, *1* (5), 575–583.
(18) Diaz, K. M.; Howard, V. J.; Hutto, B.; Colabianchi, N.; Vena, J. E.; Safford, M. M.; Blair, S. N.; Hooker, S. P. Patterns of Sedentary Behavior and Mortality in U.S. Middle-Aged and Older Adults a National Cohort Study. *Ann. Intern. Med.* **2017**, *167* (7), 465–475.
(19) Young, D. R.; Hivert, M. F.; Alhassan, S.; Camhi, S. M.; Ferguson, J. F.; Katzmarzyk, P. T.; Lewis, C. E.; Owen, N.; Perry, C. K.; Siddique, J.; Yong, C. M. Sedentary Behavior and Cardiovascular Morbidity and Mortality: A Science Advisory from the American Heart Association. *Circulation* **2016**, *134* (13), e262–e279.
(20) Graham, B. T.; Moore, A. C.; Burris, D. L.; Price, C. Detrimental Effects of Long Sedentary Bouts on the Biomechanical Response of Cartilage to Sliding. *Connect. Tissue Res.* **2020**, 1–14.
(21) Burris, D. L.; Moore, A. C. Cartilage and Joint Lubrication: New Insights Into the Role of Hydrodynamics. *Biotribology* **2017**, *12*, 8–14.
(22) Moore, A. C.; Burris, D. L. Tribological Rehydration of Cartilage and Its Potential Role in Preserving Joint Health. *Osteoarthr. Cartil.* **2017**, *25* (1), 99–107.
(23) Graham, B. T.; Moore, A. C.; Burris, D. L.; Price, C. Sliding Enhances Fluid and Solute Transport into Buried Articular Cartilage Contacts. *Osteoarthr. Cartil.* **2017**.
(24) Varady, N. H.; Grodzinsky, A. J. Osteoarthritis Year in Review 2015: Mechanics. *Osteoarthr. Cartil.* **2016**, *24* (1), 27–35.
(25) Mow, V. C.; Ateshian, G. A.; Spilker, R. L. Biomechanics of Diarthrodial Joints: A Review of Twenty Years of Progress. *J. Biomech. Eng.* **1993**, *115* (4B), 460–467.
(26) Duarte, M.; Zatsiorsky, V. M. Patterns of Center of Pressure Migration during Prolonged Unconstrained Standing. *Motor Control* **1999**, *3* (1), 12–27.
(27) Rekant, J. S.; Wiltman, S. A.; Chambers, A. J. A Novel Method of Analysis for Prolonged-Standing Data: Accounting for Joint and Muscle Discomfort. *IISE Trans. Occup. Ergon. Hum. Factors* **2019**, *7* (2), 142–152.
(28) Lewis, P. R.; McCutchen, C. W. Experimental Evidence for Weeping Lubrication in Mammalian Joints. *Nature* **1959**, *184*, 1285.
(29) Williams, P. T. Effects of Running and Walking on Osteoarthritis and Hip Replacement Risk. *Med. Sci. Sport. Exerc.* **2013**, *45* (7), 1292–1297.
(30) Voinier, D.; Neogi, T.; Stefanik, J. J.; Guermazi, A.; Roemer, F. W.; Thoma, L. M.; Master, H.; Nevitt, M. C.; Lewis, C. E.; Torner, J.; White, D. K. Using Cumulative Load to Explain How Body Mass Index and Daily Walking Relate to Worsening Knee Cartilage Damage Over Two Years: The MOST Study. *Arthritis Rheumatol.* **2020**, *72* (6), 957–965.
(31) Lane, N. E. Physical Activity at Leisure and Risk of Osteoarthritis. *Ann. Rheum. Dis.* **1996**, *55* (9), 682–684.
(32) Hootman, J. M.; Macera, C. a.; Helmick, C. G.; Blair, S. N. Influence of Physical Activity-Related Joint Stress on the Risk of Self-Reported Hip/Knee Osteoarthritis: A New Method to Quantify Physical Activity. *Prev. Med. (Baltim).* **2003**, *36* (5), 636–644.

(33) Moore, A. C.; Burris, D. L. Tribological and Material Properties for Cartilage of and throughout the Bovine Stifle: Support for the Altered Joint Kinematics Hypothesis of Osteoarthritis. *Osteoarthr. Cartil.* **2015**, *23* (1).
(34) Moore, A. C.; DeLucca, J. F.; Elliott, D. M.; Burris, D. L. Quantifying Cartilage Contact Modulus, Tension Modulus, and Permeability with Hertzian Biphasic Creep. *J. Tribol.* **2016**, *138* (4).
(35) Agbezuge, L.; Deresiewicz, H. On the Indentation of a Consolidating Half-Space. *Isr. J. Technol.* **1974**.
(36) Chen, X.; Dunn, A. C.; Sawyer, W. G.; Sarntinoranont, M. A Biphasic Model for Micro-Indentation of a Hydrogel-Based Contact Lens. *J. Biomech. Eng.* **2007**, *129* (2), 156–163.
(37) Soltz, M. A.; Ateshian, G. A. A Conewise Linear Elasticity Mixture Model for the Analysis of Nonlinearity in Articular Cartilage. *J. Biomech. Eng.* **2000**, *122* (6), 576–586.
(38) Moore, A. C.; Zimmerman, B. K.; Chen, X.; Lu, X. L.; Burris, D. L. Experimental Characterization of Biphasic Materials Using Rate-Controlled Hertzian Indentation. *Tribol. Int.* **2015**, *89*.
(39) Johnson, K. L. (Kenneth L. *Contact Mechanics*; Cambridge University Press, 1985.
(40) Roger, A. Biomechanics of Walking, Running, and Sprinting. **1979**, 345–350.
(41) Anderson, A. E.; Ellis, B. J.; Maas, S. A.; Peters, C. L.; Weiss, J. A. Validation of Finite Element Predictions of Cartilage Contact Pressure in the Human Hip Joint. *J. Biomech. Eng.* **2008**, *130* (5), 051008.
(42) Carter, M. J.; Basalo, I. M.; Ateshian, G. A. The Temporal Response of the Friction Coefficient of Articular Cartilage Depends on the Contact Area. *J. Biomech.* **2007**, *40* (14), 3257–3260.
(43) Charnley, J. The Lubrication of Animal Joints in Relation to Surgical Reconstruction by Arthroplasty. *Ann. Rheum. Dis.* **1960**, *19*, 10–19.
(44) Eckstein, F.; Hudelmaier, M.; Putz, R. The Effects of Exercise on Human Articular Cartilage. *J. Anat.* **2006**, *208* (4), 491–512.
(45) Duarte, M.; Harvey, W.; Zatsiorsky, V. M. Stabilographic Analysis of Unconstrained Standing. *Ergonomics* **2000**, *43* (11), 1824–1839.
(46) Cher, W. L.; Utturkar, G. M.; Spritzer, C. E.; Nunley, J. A.; DeFrate, L. E.; Collins, A. T. An Analysis of Changes in in Vivo Cartilage Thickness of the Healthy Ankle Following Dynamic Activity. *J. Biomech.* **2016**, *49* (13), 3026–3030.
(47) Eckstein, F.; Tieschky, M.; Faber, S. C.; Haubner, M.; Kolem, H.; Englmeier, K. H.; Reiser, M. Effect of Physical Exercise on Cartilage Volume and Thickness in Vivo: MR Imaging Study. *Radiology* **1998**, *207* (1), 243–248.
(48) Chan, D. D.; Cai, L.; Butz, K. D.; Trippel, S. B.; Nauman, E. A.; Neu, C. P. In Vivo Articular Cartilage Deformation: Noninvasive Quantification of Intratissue Strain during Joint Contact in the Human Knee. *Sci. Rep.* **2016**.
(49) Krishnan, R.; Kopacz, M.; Ateshian, G. A. Experimental Verification of the Role of Interstitial Fluid Pressurization in Cartilage Lubrication. *J. Orthop. Res.* **2004**, *22* (3), 565–570.
(50) Bonnevie, E. D.; Delco, M. L.; Bartell, L. R.; Jasty, N.; Cohen, I.; Fortier, L. A.; Bonassar, L. J. Microscale Frictional Strains Determine Chondrocyte Fate in Loaded Cartilage. *J. Biomech.* **2018**, *74*, 72–78.
(51) *Physical Activity and Health: A Report of the Surgeon General*; 1996.
(52) Wallace, I. J.; Worthington, S.; Felson, D. T.; Jurmain, R. D.; Wren, K. T.; Maijanen, H.;

Woods, R. J.; Lieberman, D. E. Knee Osteoarthritis Has Doubled in Prevalence since the Mid-20th Century. *Proc. Natl. Acad. Sci. U. S. A.* **2017**, *114* (35), 9332–9336.
(53) Gleghorn, J. P.; Bonassar, L. J. Lubrication Mode Analysis of Articular Cartilage Using Stribeck Surfaces. *J. Biomech.* **2008**, *41* (9), 1910–1918.
(54) Bonnevie, E. D.; Galesso, D.; Secchieri, C.; Cohen, I. Elastoviscous Transitions of Articular Cartilage Reveal a Mechanism of Synergy between Lubricin and Hyaluronic Acid. **2015**, 1–15.
(55) Lad, N. K.; Liu, B.; Ganapathy, P. K.; Utturkar, G. M.; Sutter, E. G.; Moorman, C. T.; Garrett, W. E.; Spritzer, C. E.; DeFrate, L. E. Effect of Normal Gait on in Vivo Tibiofemoral Cartilage Strains. *J. Biomech.* **2016**, *49* (13), 2870–2876.
(56) Liu, B.; Lad, N. K.; Collins, A. T.; Ganapathy, P. K.; Utturkar, G. M.; McNulty, A. L.; Spritzer, C. E.; Moorman, C. T.; Sutter, E. G.; Garrett, W. E.; DeFrate, L. E. In Vivo Tibial Cartilage Strains in Regions of Cartilage-to-Cartilage Contact and Cartilage-to-Meniscus Contact in Response to Walking. *Am. J. Sports Med.* **2017**, *45* (12), 2817–2823.

Captions

Figure 1 (A) Schematic of the instrument and experimental setup. (B) Top-down view and (C) side view of MCA experiments with definitions of terms. Arrows are drawn to represent fluid flows and dots are drawn at position 1 and 2 to denote locations where the cartilage is exuding and recovering, respectively, at the current probe position.

Figure 2: (A) Raw penetration depth (δ) and normal force (F) measurements versus time for a representative variable migration length experiment. The migration length varied between shaded bands as indicated above the figure. (B) Effective contact modulus (E_c), contact area (A_c) and contact stress (σ) versus time for the same representative experiment. The migration length is shown for each testing interval above both figures. Samples were loaded to static equilibrium (S = 0) at the start of each test, then slid (at 1.5 mm/s) across a 7 mm track length until its dynamic equilibrium was reached. Following dynamic equilibrium, track lengths were decreased systematically to 0.05 mm, followed by a final static equilibration at the end of the test.

Figure 3. Average values of: (A) effective contact modulus (E_c) versus migration length (S); (B) contact area (A_c) versus S; and (C) contact stress (σ) versus S for representative experiments with samples 1, 3 and 5 (properties given in Table 2). Data from individual samples are connected by straight lines for visualization of trends. The results illustrate that the mechanical response of cartilage to sliding in the MCA is sensitive to material properties and migration length. (D) The relative fluid load support (F^*) responses of these samples collapse onto a single sigmoidal curve as described by Eq. 3 when plotted versus the relative migration length (S^*). Data labels and error bars (inside of the symbols) represent the mean and standard deviation, respectively.

Figure 4. Relative *FLS* (F^*) versus relative migration length (S^*) for all 360 individual measurements in the study (8 migration lengths, 5 samples, 3 loads, and 3 probe radii). The fit to Eq. 3 gives a transition, defined at $F^* = 0.5$, of $S^* = 0.11$, which is equivalent to $R^* = 0.14$; *i.e.* the exudation rate was 14% the recovery rate.

Figure 5. Experimental fits to exudation ratio values (R^*) for each set of variable migration length experiments plotted versus (A) contact stress and (B) contact area at full fluid load support. The overall linear fits and 95% confidence intervals are shown as solid and dashed lines, respectively. Overall, the exudation ratio (R^*) increased significantly with contact stress ($p < 0.0001$), but not with contact area ($p = 0.06$).

Table 1. Definition of terms used in this study. Material properties are fit to indentation data using methods described previously[16].

Table 2. Measured material properties of the five samples used in this study listed in order of descending stiffness. The properties for each sample were quantified based on the fits to all nine creep relaxation curves (the initial 0 mm condition for each experiment). The mean and the standard deviation for the fits to these 9 independent measurements are given.

Figures

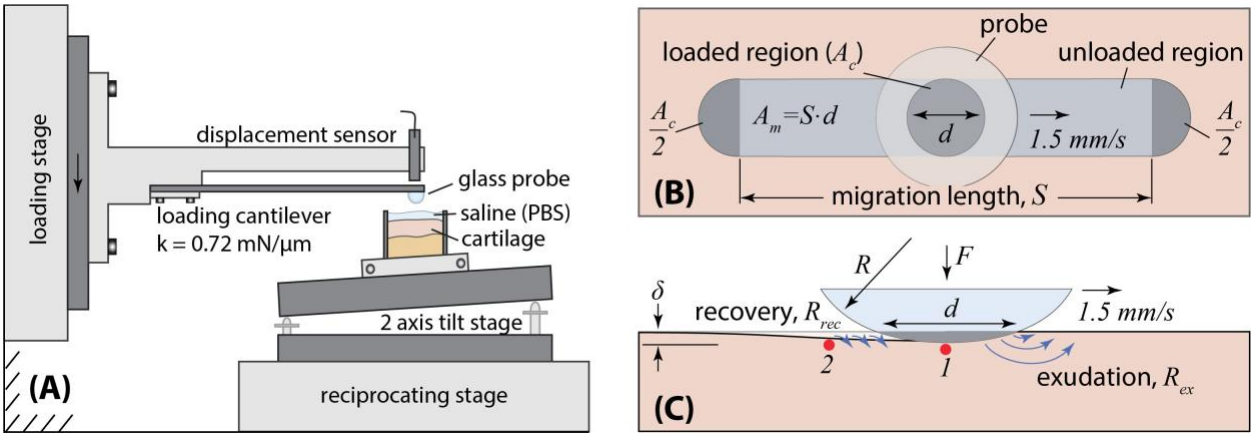

Figure 1

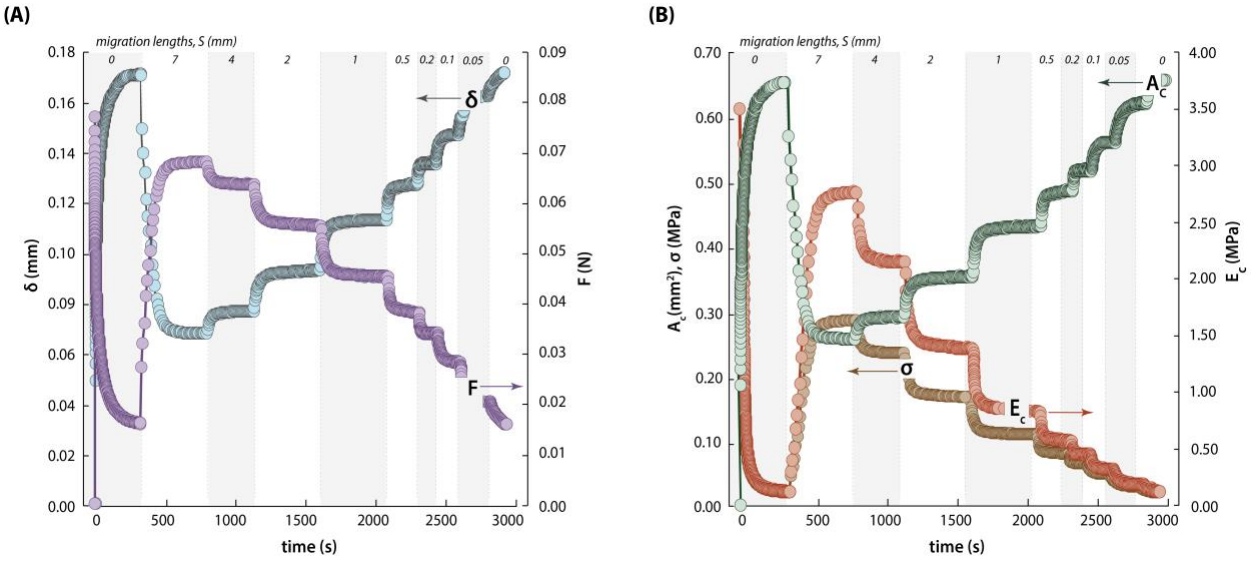

Figure 2

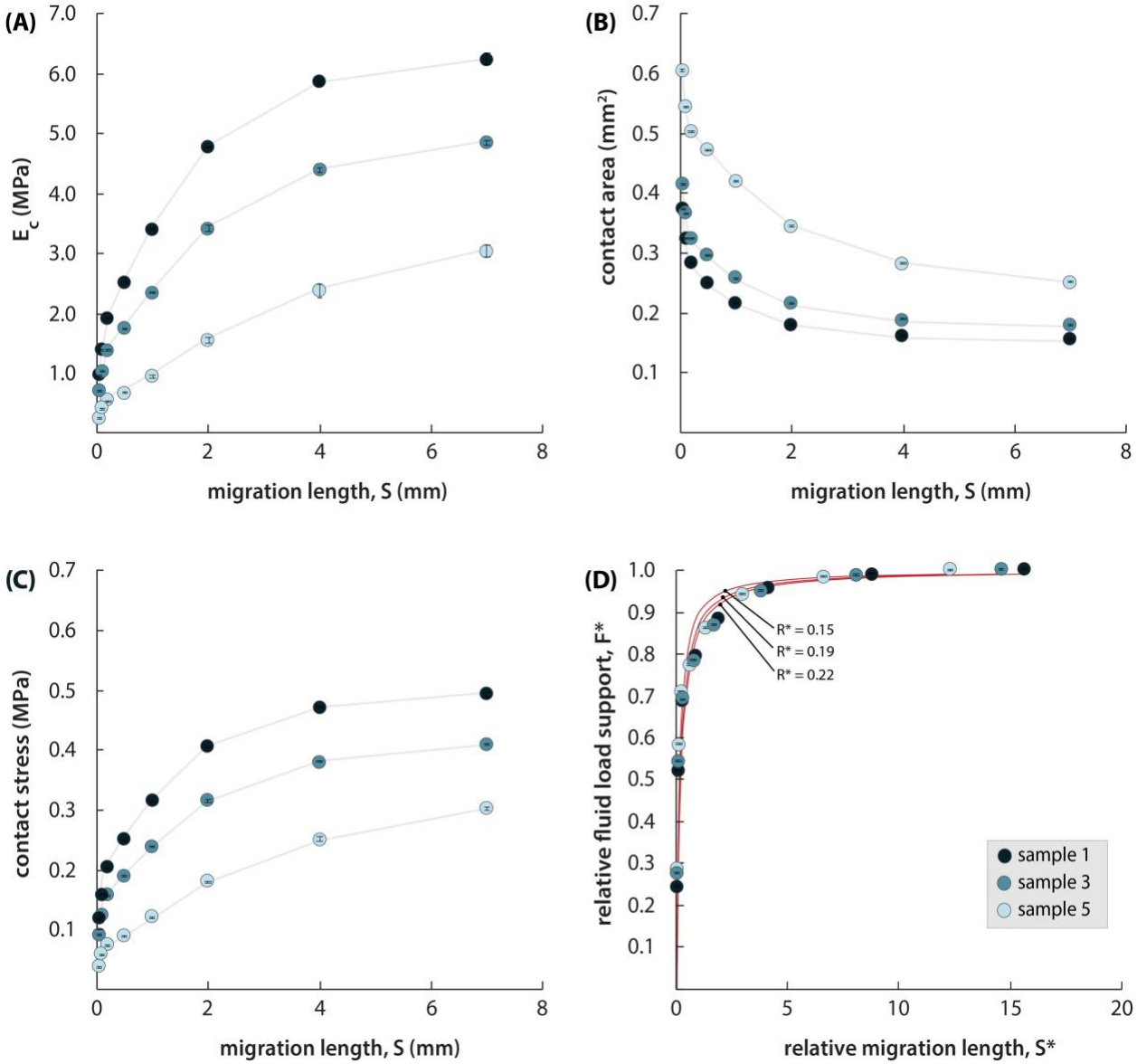
(A)
E_c (MPa)
migration length, S (mm)
(B)
contact area (mm²)
migration length, S (mm)
(C)
contact stress (MPa)
migration length, S (mm)
(D)
relative fluid load support, F*
R* = 0.15
R* = 0.19
R* = 0.22
sample 1
sample 3
sample 5
relative migration length, S*

Figure 3

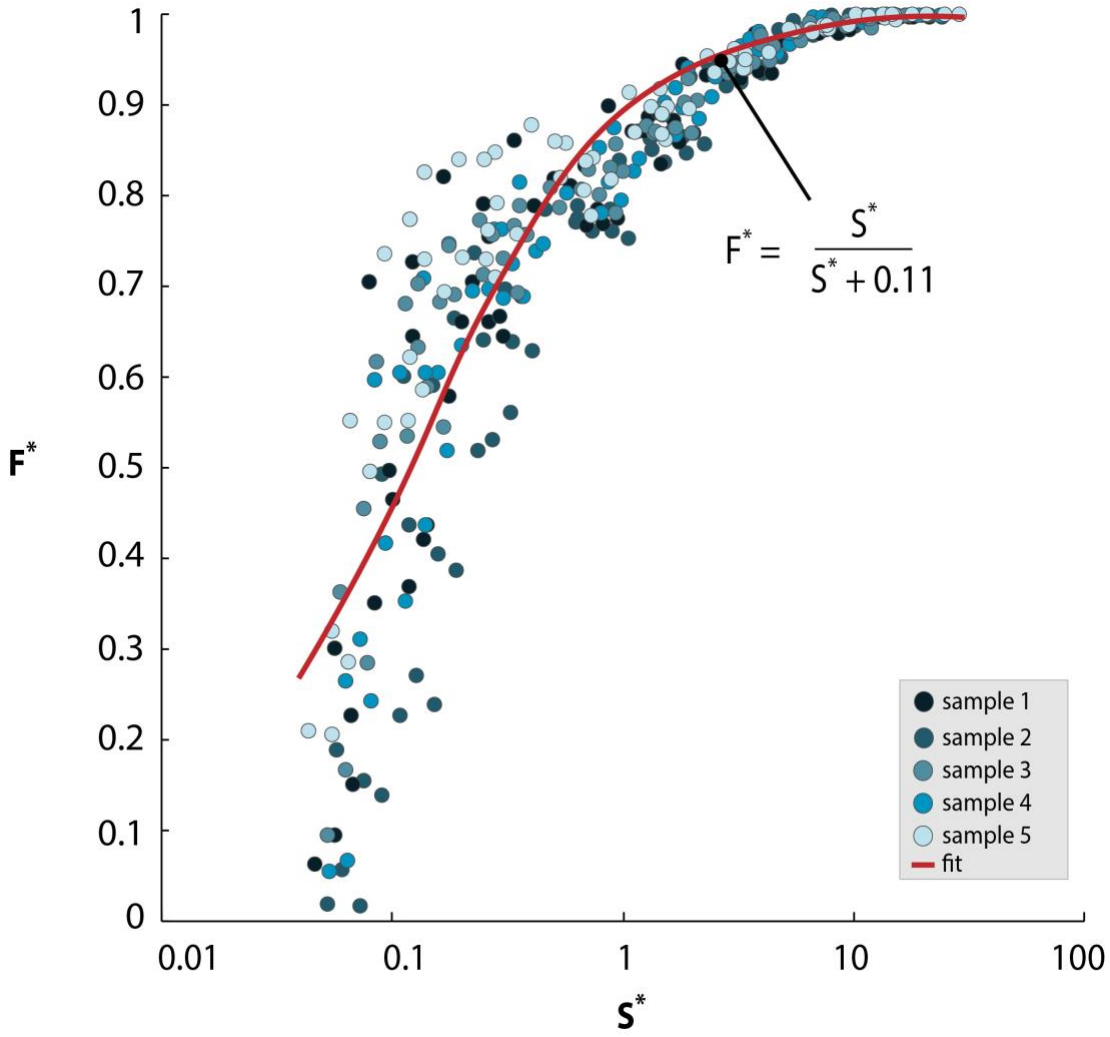
1
0.9
0.8
0.7
0.6
0.5
0.4
0.3
0.2
0.1
0
F*
0.01
0.1
1
10
100
S*
F* = S* / (S* + 0.11)
sample 1
sample 2
sample 3
sample 4
sample 5
fit

Figure 4

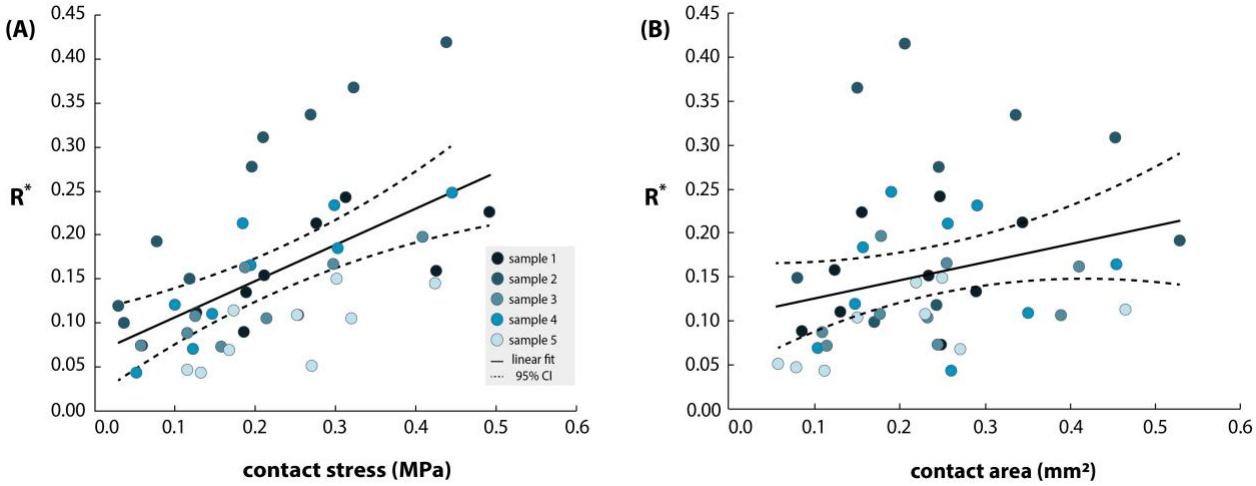
(A)
R*
contact stress (MPa)
sample 1
sample 2
sample 3
sample 4
sample 5
linear fit
95% CI
(B)
R*
contact area (mm²)

Figure 5

Tables

Table 1

Material Properties		**Mechanical conditions**	
E_{c0}	Equilibrium contact modulus	A_c	Contact area = πa^2
E_t	Tensile modulus	σ	Contact stress = F/A_c
k	Permeability	Pe	Peclet number = $(V \cdot a)/(E_{c0} \cdot k)$
Mechanical conditions		FLS	Fluid load support (FLS) = $(E_c - E_{c0})/ E_c$
F	Contact force	FLS_{max}	FLS on an infinite track
R	Probe radius	F^*	Relative $FLS = FLS/FLS_{max}$
V	Sliding speed	A_m	Migration area = $S \cdot d$
S	Migration length	A^*	Relative migration area = A_m/A_c
δ	Penetration depth	S^*	Relative migration length = S/d
a	Contact radius = $\sqrt{R\delta}$	R^*	Exudation ratio (R_{ex}/R_{rec})
d	Contact diameter = $2a$	R_{ex}	Exudation rate (varies, not quantified directly)
E_c	Effective contact modulus = $3F \cdot R/(4a^3)$	R_{rec}	Recovery rate (varies, not quantified directly)

Table 2

Sample Number	E_{c0} **(MPa)**	E_t **(MPa)**	k **(mm^4/N.s)**
1	0.83 ± 0.20	14.0 ± 4.7	0.0016 ± 0.0010
2	0.90 ± 0.28	9.4 ± 4.6	0.0019 ± 0.0010
3	0.36 ± 0.13	13.0 ± 4.8	0.0030 ± 0.0014
4	0.58 ± 0.09	9.2 ± 2.4	0.0028 ± 0.0010
5	0.20 ± 0.07	13.0 ± 8.3	0.0025 ± 0.0016